

Computational Approaches for Materials Discovery and Development Prospective



Dynamic localized phase transformation at stacking faults during creep deformation and new criterion for superalloy design

Longsheng Feng[®], and Ashton Egan, Department of Materials Science and Engineering, The Ohio State University, 2041 College Road, Columbus, OH 43210, USA

Fei Xue, and Emmanuelle Marquis, Department of Materials Science and Engineering, University of Michigan, Dow Building, 2300 Hayward St., Ann Arbor,

Michael J. Mills, and Yunzhi Wang, Department of Materials Science and Engineering, The Ohio State University, 2041 College Road, Columbus, OH 43210,

Address all correspondence to Yunzhi Wang at wang.363@osu.edu

(Received 9 April 2022; accepted 23 August 2022)

Abstract

A novel phenomenon, dynamic localized phase transformation (LPT) at stacking faults during deformation, has been observed in various Ni-base and Co-base superalloys and found to play a critical role in determining the creep performance of these alloys. In this article, we review recent experiment observations of LPT, thermodynamic analysis on the fundamentals of LPT, first-principles calculations to link LPT to mechanical deformation, and computational tools and databases required to predict LPT. We discussed the generality of the LPT phenomenon, various challenges in quantitative predictions of LPT, LPT-strengthening and LPT-softening, and opportunities offered by the LPT mechanism in the design of the next generation of LPT-strengthened superallovs.

Introduction

Recently, a new strengthening mechanism was proposed for Nibase superalloys, localized phase transformation (LPT) at stacking faults (SF).[1] It was found that either ordered or disordered phases could form just locally at the stacking faults (referred to as ordered/disordered stacking fault phases (SFP) hereafter), i.e., they do not grow into bulk forms, and different SFPs can have drastically different impacts on the creep performances of these superalloys.^[1,2] A disordered matrix could have an ordered stacking fault and the same is true vice versa. For instances, the stacking fault in FCC is naturally disordered when it is being created. But the disordered state may not be the most stable configuration, since the stacking fault has a different structure from the matrix (e.g., an HCP environment in the case of FCC). Therefore, it is possible that in the local HCP stacking environment, atoms prefer to be ordered instead of disordered. The same is true for an ordered matrix that may have a stable disordered stacking fault phase (see more detailed discussion in Computation-aided understanding of LPT). Egan et al.[3] later found that LPT can occur not only at stacking faults, but also at deformation twin boundaries, and it has similar impact on the creep performance. Feng et al. [4] explored the thermodynamic foundation of LPT, analyzed its connections to deformation and its similarities and difference from segregation transition and grain boundary complexions, and discussed its application to not only stacking faults or coherent twin boundaries but also other defects with unique local structures and the corresponding solute-defect interactions.^[4]

In this article, using stacking faults as an example, we first review the experimental observations of various LPTs in the

 γ' phase in Ni-base superalloys. We then examine how computational tools have been used to understand and rationalize the LPT phenomenon and how LPTs could be utilized in alloy design to achieve significantly improved creep properties. Finally, we discuss the challenges and opportunities in this area, especially how advanced computational modeling methods could aid more accurate quantitative prediction of the phenomenon and resolve some of the issues that are still puzzling us.

Experimental observation of LPTs at stacking faults

Observations of LPTs have been primarily conducted via high resolution scanning transmission electron microscopy (HR-STEM) based techniques, namely high angle annular dark field (HAADF) imaging to observe the structure with Z-contrast and energy-dispersive X-ray spectroscopy (EDS) to determine the local compositions. [1-3,5-8] In addition, atom probe tomography (APT) has also been utilized for compositional analysis of various SFPs and Cottrell atmospheres surrounding the associated partial dislocations.^[9,10] Both techniques have drawbacks that the other complements. Site occupancies are more readily elucidated via atomic-scale EDS and an example of a STEM EDS analysis of a superlattice-intrinsic-stacking-fault (SISF) in alloy TSNA1^[8] is given in Fig. 1. However, STEM EDS analyses may not be able to capture accurate segregation at SFPs, likely due to the inaccuracies inherent in the correction methods used in



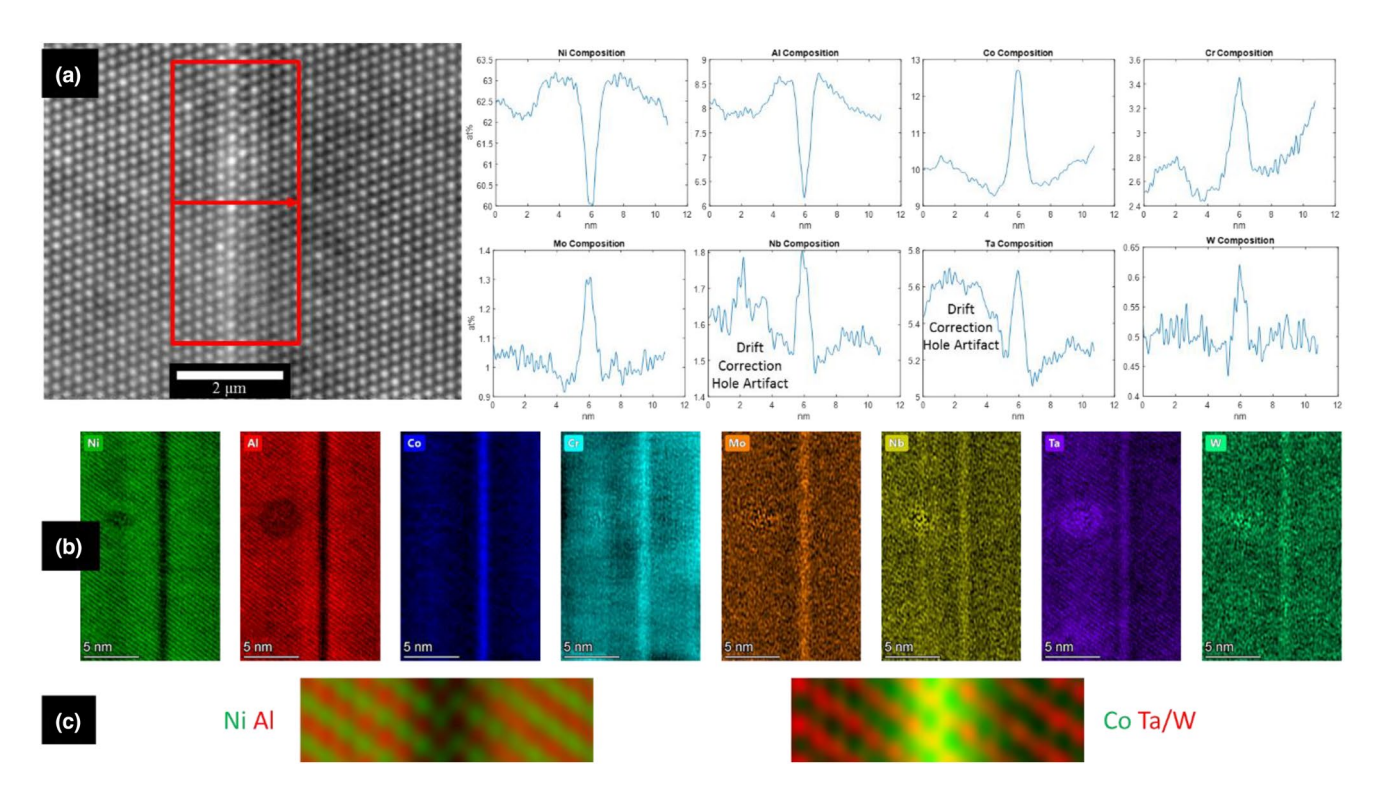


Figure 1. (a) Probe-corrected STEM image of χ -SISF in TSNA1 with corresponding EDS line-scans. (b) EDS composition maps of the SISF. (c) Vertically integrated SISF EDS map elucidating sublattice preferences for key elements at a similar SISF, adapted from Ref. 8.

EDS, [11,12] while APT may avoid this issue as it does not rely on correction factors and in theory provides direct elemental quantification. Additionally, atom probe can assess the homogeneity of solutes, which corresponds to LPT ordering along the fault plane. Although varying degrees of ordering have been reported in STEM, this is only an assessment of average atomic number down atomic columns; little information is gathered about the solute distribution along the along faults plane to understand the ordering evolution. Therefore, APT is a powerful tool in complement to STEM to investigate the chemistry in 3-D, and specifically the chemical environment resulting from dislocation-precipitate interactions to help propel the study of LPT kinetics and inform computational studies. For example, APT more readily highlights the three dimensionality of interfacial morphologies in Fig. 2, in addition to providing more details about the segregation distribution along the faults. The so-called "notches" are well delineated spatially at interface with clear connection

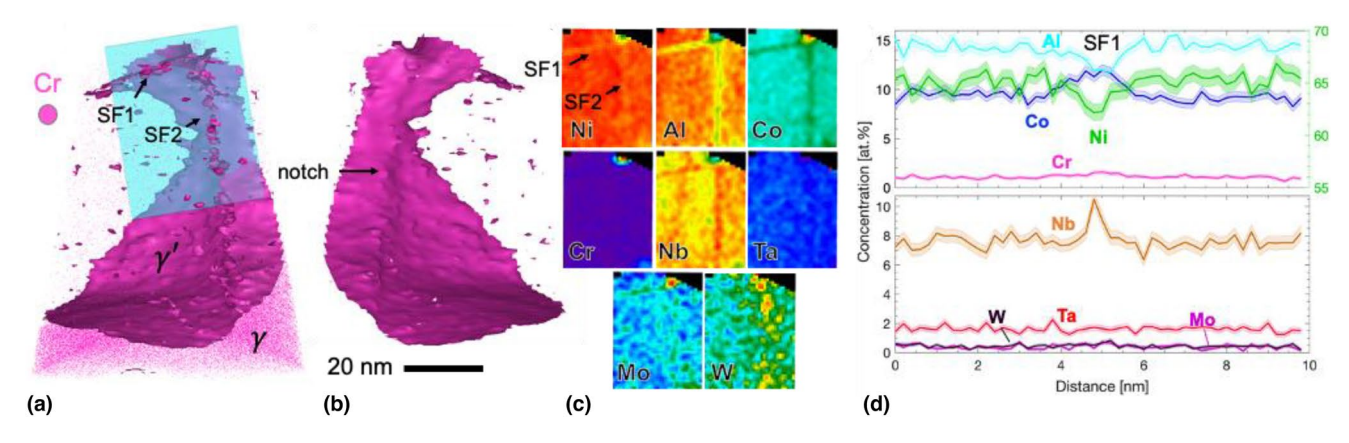


Figure 2. APT analysis of a tip showing two SFs in a < 011 > -SISF-oriented grain RRHT5[15] at 0.5% strain after compressive creep test. (a) atomic reconstruction with part of Cr atoms and γ/γ' interface delineated by 14 at.% (Cr+Co) iso-concentration surface; (b) 180° rotation of atomic reconstruction along tip axis without Cr atoms, showing a notch connecting SF2; (c) 2D maps of Ni, Al, Co, Cr, Nb, Ta, Mo, and W on a 44 nm slice containing two SFs indicated by a blue box in (a); (d) 1d profile across SF1 integrated by a Φ 28×19×10 nm³ cylinder.

to two SFs in γ' . Creation of the notch is a key component of shearing γ' by dislocations cutting the precipitates since it initiates solute diffusional processes that enable partial dislocation motion and notably, the reduction of stacking fault energies by creation of γ -like atmosphere in γ' at interfacial dislocations. Previously, these notches created at γ' interfaces have only been briefly studied with STEM EDS in the <011> zone axis in 2-D.[14] However, no observations of the diffusion field along the "pipe" of these dislocations have been reported, at both initiation or during shearing. With such advantage for chemistry characterization, one should note that APT is limited in spatial resolution, and the trajectory aberrations at interfaces can lead to limited accuracy.[13] In addition, APT often suffers from the lack of direct atomic structural information, so without carefully correlated S/ TEM analysis, the nature of the studied defects often remains ambiguous.

The most prominent examples of LPT at stacking faults are observed in the γ' phase [L1₂ crystal structure, Fig. 3(a)] in various Ni-base and Co-base superalloys. The stacking faults associated with the LPT phenomenon are superlattice-intrinsic-stacking-fault (SISF) and superlattice-extrinsic-stacking-fault (SESF). The SISF in L1₂ is a single-layer fault with a local D0₁₉ crystal structure [its bulk counterpart is the χ phase, Fig. 3(e)] created by dislocations with a combined Burgers vector of $\frac{1}{3} < 11\overline{2} >$, which is commonly composed of three Shockley partials. [16] The SESF in L1₂ is a two-layer fault with a local D0₂₄ crystal structure (its bulk counterpart is the η phase, Fig. 3(j)) created by two identical Shockley partials shearing adjacent (111) planes (pseudo-twin) followed by a reordering process to eliminate the high-energy Al-Al bond. [17] On both the SISF and SESF, there can be disordered counterparts of the

ordered SFPs, e.g., HCP for χ and dHCP for η , [18] enabled by order–disorder transitions at the stacking faults.

Figure 3(b) shows a $[1\overline{1}0]$ projection of the γ' crystal structure, which is commonly used to view the stacking faults in the STEM experiments (i.e., observation via <011> zone axis, Fig. 1). The full orange circles represent the Ni-sublattice and the half-green and half-orange circles represent a combined Niand Al-sublattice in the two different types of atomic columns shown in the figure. Figure 3(c) shows the same projection after an SISF has formed and a zigzag pattern in the red box is highlighted. Since heavy elements like Mo, Nb, Ta, and W occupy the Al-sublattice^[19–21] and show significant contrast in HAADF imaging, the zigzag pattern can be a good indicator of whether the heavy elements segregate at the Al sites, forming a local x phase [Fig. 3(d)]. Similarly, Fig. 3(f-h) show the $[1\overline{1}0]$ projections of the perfect γ' crystal structure, pseudo-twin, and SESF structure. The Al-Al bond boxed in red in Fig. 3(g) indicates the high-energy pseudo-twin and the need for reordering to lower its energy, resulting the formation of SESF. Another zigzag pattern is highlighted in Fig. 3(h) for SESF, which can be a good indicator of whether a local η phase has formed [Fig. 3(i)]. In addition to the atomic scale observations, the <011> zone axis HAADF imaging at low magnifications also reveals LPT and is a useful surveying tool. At this scale, these appear as bright line traces due to the accumulation of heavy species on the {111} planes of the defect, and comparison of the same region utilizing a high camera length (diffraction contrast imaging) can quickly determine the presence/absence of LPT relative to the entire defect structure.

The chemical segregation associated with different SFPs varies based on the defect type. Tables I and II summarize the solutes observed to segregate to SISF and SESF in various

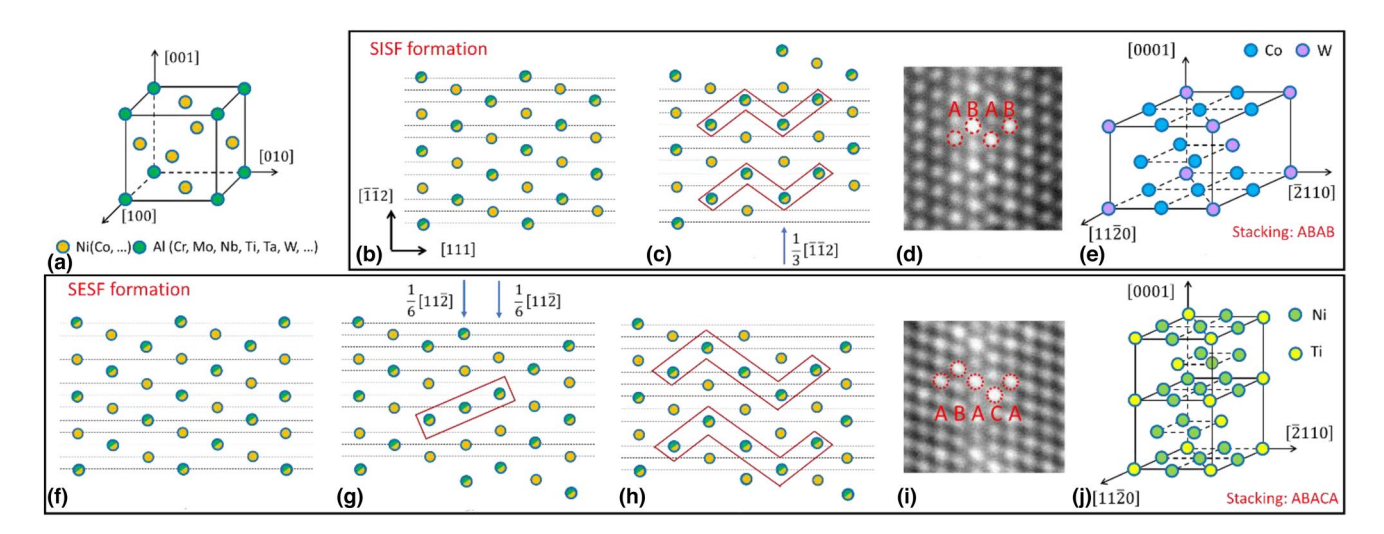


Figure 3. (a) Crystal structure of the γ' phase with Ni and Co occupying the Ni-sublattice and Al and the rest (and most heavy) elements occupying the Al-sublattice. (b) Stacking sequence and $\begin{bmatrix} 1\overline{1}0 \end{bmatrix}$ projection of the γ' phase. (c) SISF formation with a total of $\frac{1}{3}\begin{bmatrix} 112 \end{bmatrix}$ displacement on a (111) plane. (d) HAADF image of the SISF with χ phase formation, adapted from Ref. 4 (e) D0₁₉ (χ) crystal structure with chemical prototype of Co₃W. (f) Stacking sequence and $\begin{bmatrix} 1\overline{1}0 \end{bmatrix}$ projection of the γ' phase. (g) Pseudo-twin formation after two identical Shockley partials shearing on adjacent [111] layers. (h) SESF formation from pseudo-twin after reordering. (i) HAADF image of the SESF with η phase formation, adapted from Ref. 4 (j) D0₂₄ (η) crystal structure with a chemical prototype of Ni₃Ti



Table I. Segregation behavior of different solutes at SISF in different Ni-base superalloys.

| Alloy | Fault | SFP | Ni | Al | Co | Cr | Nb | Ti | Ta | W | Mo |
|-------------------------|-------|-----|----|----|----|----|----|----|----|---|----|
| ME3 ^[18] | SISF | НСР | _ | _ | + | + | o | o | 0 | 0 | О |
| RRHT3 ^[15] | SISF | χ | _ | _ | + | + | + | × | × | × | + |
| LSHR ^[2] | SISF | χ | _ | _ | + | + | + | o | o | + | + |
| RRHT5 ^[3,15] | SISF | χ | _ | _ | + | + | + | × | × | × | + |
| TSNA1 ^[8] | SISF | χ | _ | _ | + | + | + | + | + | + | + |
| CMSX4 ^[14] | SISF | χ | _ | _ | + | + | × | × | × | + | + |

[&]quot;+" is for segregation, "-" for depletion, "o" for no apparent segregation pattern, and "x" means either the alloy does not have this element, or this element was not included in the analysis.

Table II. Segregation behavior of different solutes at SESF in different Ni-base superalloys.

| Alloy | Fault | SFP | Ni | Al | Со | Cr | Nb | Ti | Та | W | Mo |
|-------------------------|-------|-------------|----|----|----|----|----|----|----|---|----|
| ME3 ^[18] | SESF | dHCP | _ | _ | + | + | О | О | o | О | 0 |
| RRHT3 ^[15] | SESF | dHCP | _ | _ | + | × | × | × | × | × | × |
| LSHR ^[2] | SESF | $dHCP/\eta$ | _ | _ | + | o | + | + | o | + | + |
| RRHT5 ^[3,15] | SESF | η | _ | _ | + | o | + | × | × | × | × |
| TSNA1 ^[8] | SESF | η | _ | _ | + | + | + | + | + | + | + |
| ME501 ^[1,5] | SESF | η | _ | _ | + | o | + | + | + | + | × |

The symbols adopt the same meanings as those in Table I.

Ni-based superalloys. The corresponding SFPs are also provided. Overall, Ni and Al are depleted from while Co segregates at both SISFs and SESFs, irrespective of the type of the SFPs. At SISFs, the main χ-phase formers are Cr, Nb, Mo and W while the main HCP-phase former is Cr. Even though Ta and Ti are also observed to segregate at SISF in some of the alloys and form x phase, the enrichment amounts are small as compared to other χ -formers. At SESF, the main η -phase formers are Co, Nb, Ti, and Ta, while the dHCP-former is Co. Even though W and Mo can also segregate at SESF and form the η phase, their enrichment amounts are also small as compared to other η -formers. From this summary, it is readily seen that Co and Nb combined can promote both χ and η formation at SISF and SESF, respectively, while other solutes have different segregation behaviors at different faults. Another feature in chemical segregation across the SFPs is a local depletion zone adjacent to the stacking fault (Fig. 1), which was predicted by Feng et al. [22] but was not verified by the STEM/EDS at the time. With that modeling insight, probe-corrected STEM was later used to perform atomic-resolution EDS on χ - and η -SFPs in TSNA1, as in Fig. 1, matching the computational results.

Smith et al.^[1] compared the creep performances of several Ni-base superalloys with different LPTs and found that alloys with ordered SFPs tend to have superior creep performance than those with disordered SFPs, and also alloys with both χ and η SFPs perform better than those with just χ or η SFP. This is a clear indication that ordered SFPs have a better creep resistance than that of disordered SFPs. It has also been noticed that ordering of SFPs may appear "patchy" along the trace of the

faults (within the fault plane), i.e., a mixture of ordered and disordered SFPs, due to local fluctuation in χ/η formers. The SFP motif is pronounced and repeats (i.e., a true phase) in alloys with superior strength like TSNA1 or RRHT5. Juxtaposed are " γ -softened" alloys, in which similar contrast between Al and Ni sites indicating disordering.

Substantial investigations of similar SISF formation and related χ -LPT have also been conducted for Co-base superalloys, as these SFs are particularly of interest due to comparable anti-phase boundary (APB) and SISF energies relative to the Ni-based alloys. [9,10,23–29] Experimental studies in this family of alloys have also elucidated that both χ and η SFPs are potent strengtheners, [30] similar to those seen in Ni-based alloys.

Similar segregation and ordering behavior have been observed at deformation and annealing twin boundaries in the γ' phase as well, where the local twin boundary has a three-layer HCP stacking sequence and a localized χ phase was observed at the twin boundaries. Ni-base superalloys with χ -strengthened twin boundaries also exhibit enhanced creep performances. [3] On the other hand, despite the formation of χ as a bulk phase in Co-base superalloys, [26,31] it has not been assessed how or if χ phase affects deformation in the SESF/microtwinning mode. Though studies have noted LPT-like segregation at the microtwins, [23] no experimental work in Co-base alloys have focused on this.

The impact of LPT on mechanical properties is not confined solely to creep deformation, it may impact any deformation under a condition with sufficient combination of time (\alpha strain rate) and temperature that allow for transport of solutes along

dislocations. Experimental results of tensile tests at high temperature and constant intermediate strain rate (10⁻⁵) showed several transitions of operating deformation mechanisms from classic, athermal APB shearing (<400°C) to thermally activated (diffusion-mediated) shear of superlattice stacking faults, APBs, and microtwinning with increasing temperature. [6] Barba et al. [6] noted substantial LPT at all stacking faults for temperatures exceeding 400°C in alloy MD2 and proposed that this transition was due to increased Co diffusivity and thus formation of γ-SFP at APB, superlattice stacking faults, and microtwins.

Computation-aided understanding

Stacking faults and deformation twin boundaries have unique stacking sequences that are different from that of the matrix phase. Within each stacking fault, atoms rearrange themselves such that the stacking fault energy is minimized. Therefore, SFPs have well-defined crystal structures, which should have their own free energy curves as a function of compositions. However, the SFPs are embedded in a matrix and thus their equilibrium conditions are always confined by the surrounding matrix phase that serves as a reservoir of chemical species. In this regard, a SFP is different from a bulk equilibrium phase whose equilibrium composition is determined by the common tangent construction in a multi-phase field of a phase diagram. The uniqueness of LPT at stacking faults resides in both the unique structure of the stacking fault and the constrained equilibrium from the surrounding matrix. On one hand, with unique crystal structure, it is possible for stacking faults to undergo phase transformations, the most common of which is order-disorder transition and segregation transition.^[32-35] On the other hand, the constrained equilibrium determines the equilibrium composition of the SFP by a parallel tangent construction (constant diffusion potential) rather than the common tangent construction (constant chemical potential).

Here we give a simple example for an order-disorder transformation coupled with solute segregation at an intrinsic stacking fault (ISF) in an FCC solid solution. Figure 4 shows the schematic free energy curves of the associated phases and the transformation pathway. G_{FCC}^{Bulk} is the free energy of the matrix FCC phase and G_{Other}^{Bulk} is the free energy of other bulk phases (if any). The ISF can be a disordered HCP phase or one of its ordered counterparts, χ phase, whose free energies are represented by G_{HCP}^{ISF} and $G_{\chi}^{ISF},$ respectively. The matrix FCC phase has a composition "A", which is determined by either the alloy composition for a single-phase alloy or the common tangent construction of two-phase equilibria if there are other bulk equilibrium phases (G_{Other}^{Bulk}) present in the system. From dislocation dissociation, an ISF (1), from "A" to "B") with local HCP stacking sequence is created. The local ISF could then go through a disorder-order transition and become an ordered SFP, χ (②, from "B" to "C"), because the χ SFP has a lower energy than the HCP SFP, which is then

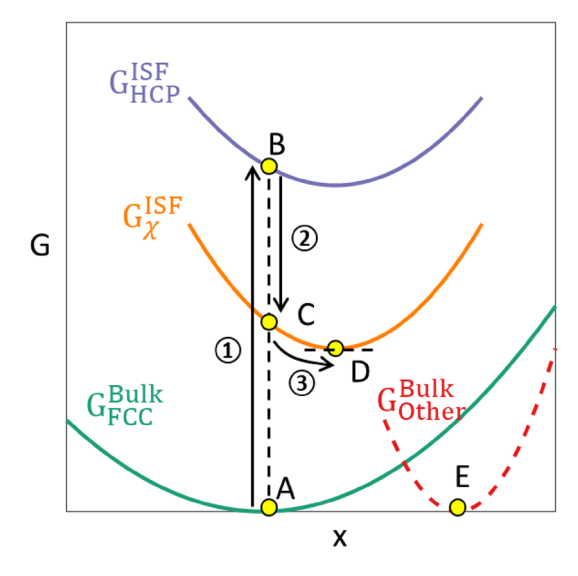


Figure 4. Schematic illustration of phase transformation pathways for the formation of an ordered stacking fault phase at ISF in an FCC solid solution. See text for the details of the transformation pathway represented.

followed by Suzuki segregation^[36,37] (③, from "C" to "D") with the equilibrium composition of the SFP determined by the parallel tangent construction with respect to that of the FCC matrix. Note that the parallel tangent at "D" with respect to "A" is also parallel to the common tangent between "A" and "E", since the common tangent determines the phase compositions in multi-phase materials. The ordering of ISF will occur only if $G_{\chi}^{ISF} < G_{HCP}^{ISF}.$ If $G_{\chi}^{ISF} > G_{HCP}^{ISF},$ the ISF will remain as a disordered phase (i.e., HCP). The same can be said for an ordered matrix phase such as γ' , where the SISF and SESF can have either ordered SFPs such as χ and η or disordered SFPs such as HCP and dHCP, just as what have been observed in the experiments.^[1,2] In general, the quantity GSF — GSF can be a good parameter to determine what SFP appears at a stacking fault, where "SF" indicates the type of stacking faults (like ISF, ESF, ...), "DIS" represents the disordered phase with the same stacking sequence as the stacking fault (e.g., HCP for ISF), "ORD" represents the ordered phase with the same stacking sequence as the stacking fault (e.g., χ for ISF), and G_{DIS}^{SF} and G_{ORD}^{SF} are the free energies of the disordered and ordered SFPs, respectively.

As mentioned earlier, ordered SFPs can be beneficial and disordered SFPs can be detrimental to the creep performance of Ni-base superalloys. This is because the ordered SFPs tend to have large shearing resistance to dislocations and thus make further shearing of the γ' precipitates harder.^[4] The SISF is commonly associated with stacking fault ribbon formation, [28,38-40] in which the SISF is trailed by an APB created by a Shockley partial shearing the SISF on the same (111) plane. The SESF is commonly associated with microtwin formation, in which identical Shockley partials shear adjacent (111) planes of the SESF consecutively. Feng et al. [4] showed



that both the in-plane and out-of-plane shear resistance would increase if ordered SFPs form at SISF and SESF. Smith et al. [1] also shows that the formation energy of twins at an η -decorated SESF in alloy ME501 is much higher than that at SESFs without the η phase. Therefore, the formation of ordered SFPs is referred to as LPT-hardening whereas the formation of disordered SFPs is referred to as LPT-softening. [4]

It is readily seen from the analysis in Fig. 4 that the free energy difference between the ordered and disordered SFPs, GSF - GSF or a critical thermodynamic parameter that can be used to predict the types of SFPs at a given a stacking fault. However, the free energies of the SFPs are not easy to acquire, especially for multicomponent systems like the superalloys. What are readily available are bulk thermodynamic databases that have been developed for Ni-base superalloys for decades. Therefore, instead of evaluating the accurate free energy difference among these SFPs, we evaluate the free energy difference of their bulk counterparts as a rough estimate, i.e., $G_{DIS}^{Bulk}-G_{ORD}^{Bulk}$. In the example shown in Fig. 4, we can evaluate $G_{HCP}^{Bulk}-G_{\chi}^{Bulk}$ instead of $G_{HCP}^{ISF}-G_{\chi}^{ISF}$, which now does not represent the absolute stability of the SFPs, but rather the ordering tendency for the ordered χ structure as compared to its disordered counterpart, i.e., HCP. This treatment will enable us to use the well-developed thermodynamic database. The difference between the SFP and its bulk counterpart may come from the small thickness of the SFP, which is easily influenced by the surrounding matrix and, thus, the interfacial energy between the SFP and matrix phase are critical to assess the free energy of the SFP. Nonetheless, the bulk counterpart should capture the multicomponent interaction that is crucial in superalloys and give qualitative trends, i.e., the larger the $G_{HCP}^{Bulk}-G_{\chi}^{Bulk}$ is, the more stable the bulk χ phase is relative to the bulk HCP phase, the more likely to have ordering than disordering at a given HCP stacking, and, thus, more likely to have an ordered SFP than a disordered SFP at an ISF. Following this reasoning, Feng et al. $^{[4]}$ evaluated the ordering tendency of the η phase at SESF using the PanNi2020 database and the result matches the creep performances of several existing Ni-base superalloys with different LPT behavior observed in the experiments.

Computation-aided alloy design with LPT-hardening

Besides the ordering tendency, there are other microstructural and material parameters that also contribute to the overall creep performance, such as the volume fraction of γ' phase and lattice misfit. Some parameters are crucial for alloy processing, such as η solvus temperature. We evaluated the abovementioned parameters using PanNi2020 database in a pseudo-binary Ni-X (X=Al, Co, Cr, Nb, Ti, Ta, Mo, and W) system for multicomponent alloys, with the content of all alloying elements except X kept the same as the best LPT-hardened alloy so far, TSNA1, [41] i.e., treating Ni as solvent and every other element as an individual solute and calculate the above-mentioned parameters as well as ordering tendency with respect to the solute content X with TSNA1 as a reference.

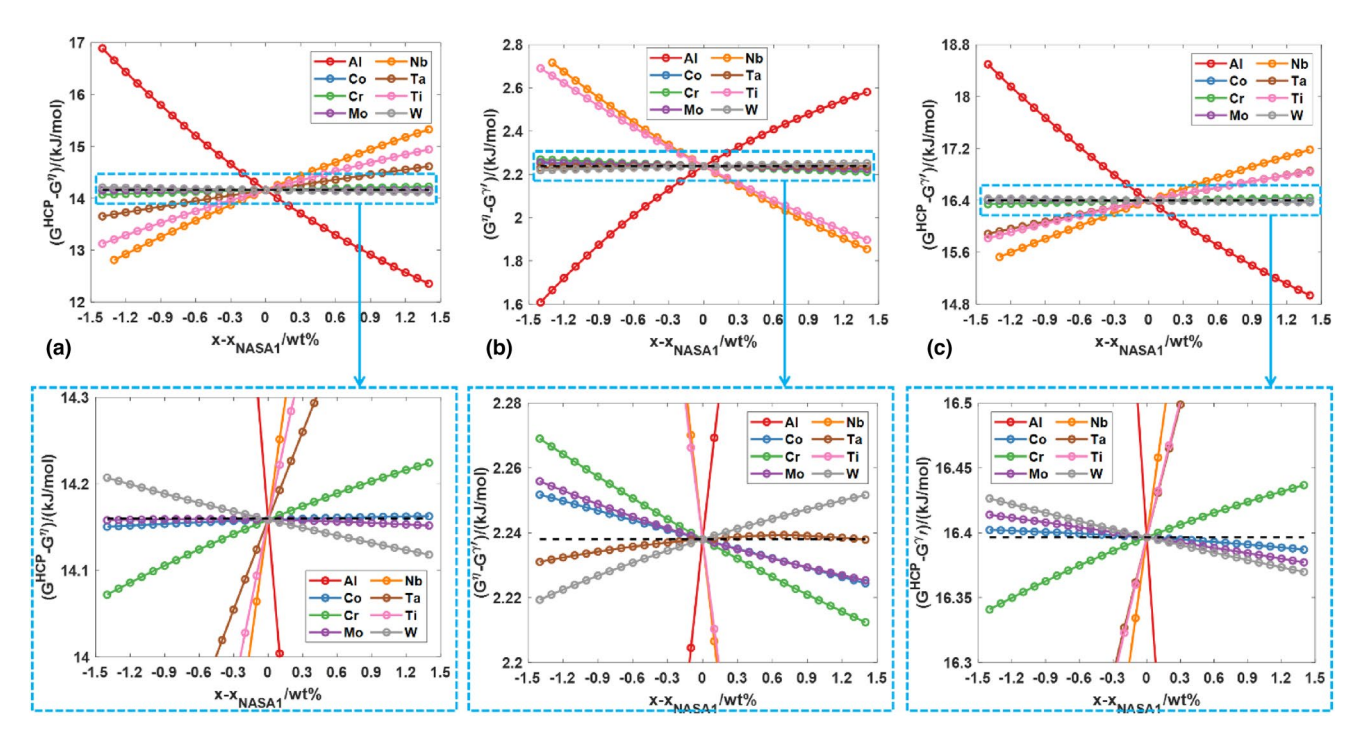


Figure 5. (a) Ordering tendency, (b) stability of η phase relative to γ' , and (c) stability of HCP phase relative to γ' phase as a function of various solutes content in the alloy.

Figure 5(a) shows the ordering tendency as a function of various solute contents in the system. The ordering tendency is most sensitive to changes in the Al content in the system and it is the only element that decreases the ordering tendency significantly with an increasing amount. For the η forming element Nb, Ti, and Ta, all of them increases the ordering tendency, but Nb is the most effective one while Ta is the least effective one. Figure 5(b) and (c) shows the relative stability of η and HCP phases with respect to the γ' phase. Interestingly, Nb and Ti lead to higher ordering tendency because both stabilize η but destabilize HCP in the γ' phase, whereas Ta has little effect on stabilizing η but very effective in destabilizing HCP in γ' . This makes Ta a preferred candidate for promoting η -hardening because it does not alter the bulk stability of η relative to γ' while Ti and Nb do, potentially avoiding the formation of bulk η phase.

Figure 6(a) shows the volume fraction of γ' phase as a function of solute content in the alloy. A larger γ' volume fraction is preferred for a stronger LPT-hardening effect, where Al, Ti, and Nb are the first three most effective elements. Figure 4(b) shows the lattice misfit between γ and γ' phases with varying alloying elements. All elements increase the misfit, which would provide additional strengthening effect if the γ' precipitates remain coherent with the γ matrix, with Nb, Ti, and Ta/Cr being the most effective. Figure 6(c) shows the effects of different solutes on η solvus. Nb and Ti significantly increase η solvus, Al significantly decreases it, while Ta has a negligible effect. It should be noted that all the calculations in Figs. 5 and 6 are direct calculations from the thermodynamic database, which captures the Gibbs free energies of different phases, the volume fraction of the γ' phase, molar volumes of different phases (used for misfit calculation) and n solvus in the multicomponent alloying space. The variations are able to demonstrate how sensitive each parameter is when different alloying elements vary with respect to the composition of NASA1. Since the topology of all the energy/volume surfaces in the hyper-dimension compositional space can be quite complicated and many local minima can exist, the conclusions we arrive based on Figs. 5 and 6 only work in the compositional space that is close to that of NASA1. But the sharp turn of Al

and Ti curve on the lattice misfit trend (Fig. 6) is unphysical, most likely caused by an artifact of the database.

From the analysis above, we have the following suggestions on promoting η -hardening with respect to alloy composition: (1) High Ta is favored. Ta increases ordering tendency and has little effect on η solvus and η stability. This will help avoid bulk η phase and also keep the η solvus temperature from being too high. (2) Medium Nb is favored. Nb is the most effective element in promoting η -hardening and increasing the misfit. But it will further stabilize bulk η and increase η solvus. (3) Low Ti is required. To maintain a $\gamma - \gamma'$ two-phase microstructure with already large amount of Nb and Ta, Ti needs to be low.

The above analysis can be further integrated into a computation framework with existing thermodynamic databases, as shown in Fig. 7. The framework has two modules: (1) conventional alloy design process where precipitate phases, volume fraction, solvus temperature, lattice misfit, etc. are screened; (2) SFP stability or ordering tendency optimization where SFP stability (if the SPF free energy database is available) or the ordering tendency (if we only have bulk thermodynamic database) are evaluated and optimized for the alloys from Module 1.

Challenges and opportunitiesDeveloping free energy database for SFPs

The biggest challenge to accurately predict LPT and thus use it for alloy design is the lack of free energy databases of different SFPs in multicomponent systems. We have been using the bulk thermodynamic database to estimate the free energies of the SFPs, but there are many limitations of this approach. The bulk counterparts of the SFPs may be metastable or unstable and thus are often not included in the thermodynamic databases. For instances, the bulk counterpart of SISF in γ' , the χ phase, is not an equilibrium phase in Ni-base superalloys. Similarly, the bulk counterpart of ESF, the dHCP phase, is rarely observed in bulk form and only a handful of rare-earth elements possess this structure (like La, Am, Nd, etc.). The lack of free energy data of these phases in the database makes it impossible to evaluate the ordering tendency. Therefore, there is an

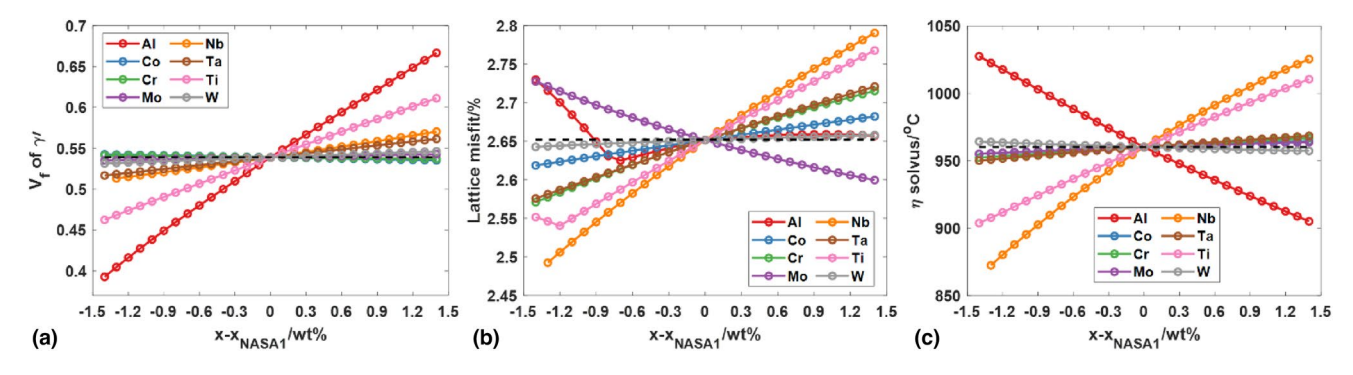


Figure 6. (a) Volume fraction of γ' , (b) Lattice misfit between γ and γ' phases, and (c) η solvus temperature as a function of various solute contents in the alloy.



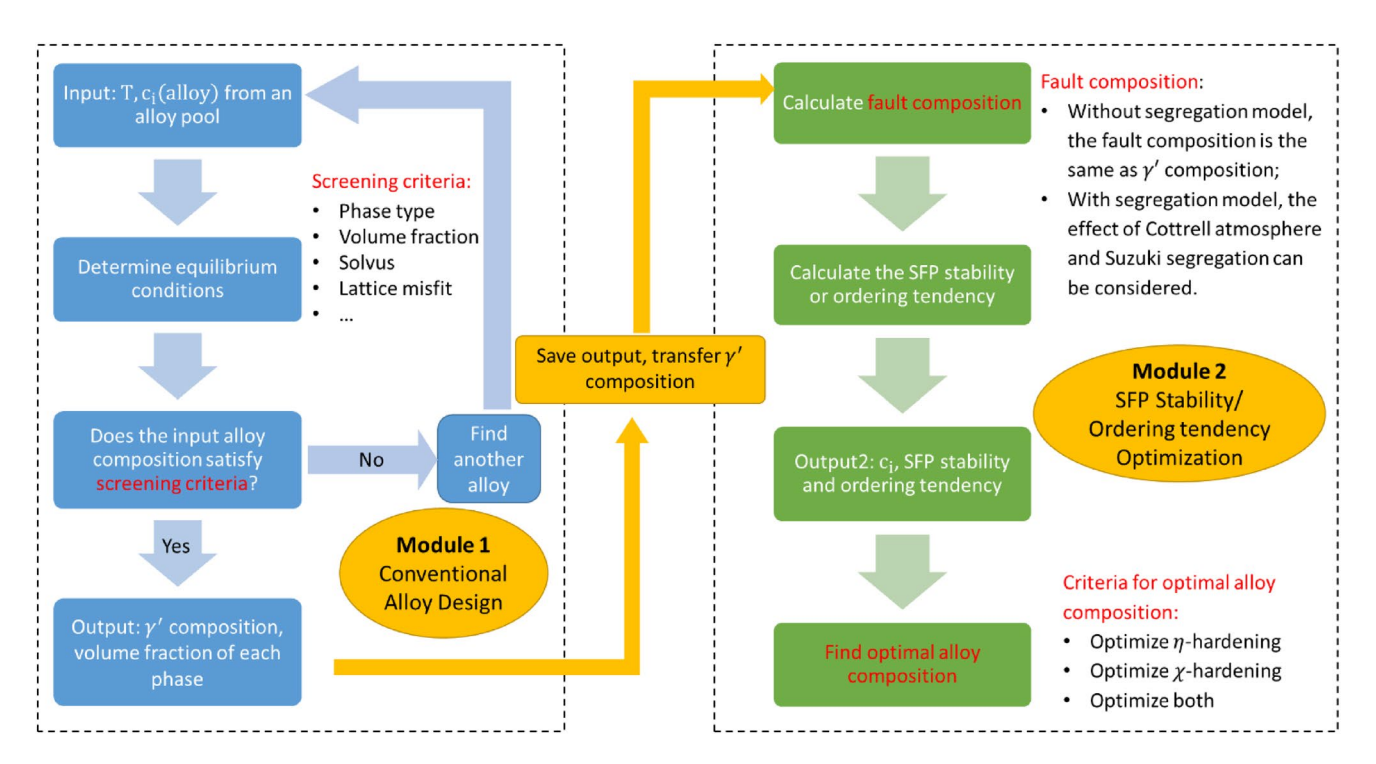


Figure 7. Computational alloy design framework incorporating LPT-hardening.

urgent need to develop a free energy database for SFPs. With the advancement of *ab initio* calculations and machine-learning (ML) atomic potentials, it is possible to calculate the free energies of SFPs as function of alloy composition for multicomponent systems at multiple temperatures. There are already many works done in binary and ternary systems, [42–50] but the data is not well-integrated and it is still computationally expensive for multicomponent systems. It might be useful if an open-source platform (like the Materials Project^[51]) can be established to gather all the calculations that have been done and can further integrate future contributions from researchers all around the

world. Meanwhile, advancement of computational methods is also necessary. Recently, Vamsi et al.^[52] found that instead of using a supercell, structure surrogates for SFPs can be used in calculating the stacking fault energy, so that the computational time can be reduced significantly. Meanwhile, the development of ML algorithms for database development may further reduce the computational cost and help build the free energy database. These ML algorithms have been used to build thermodynamic databases for various austenitic steels and complex concentrated alloys.^[53–56]

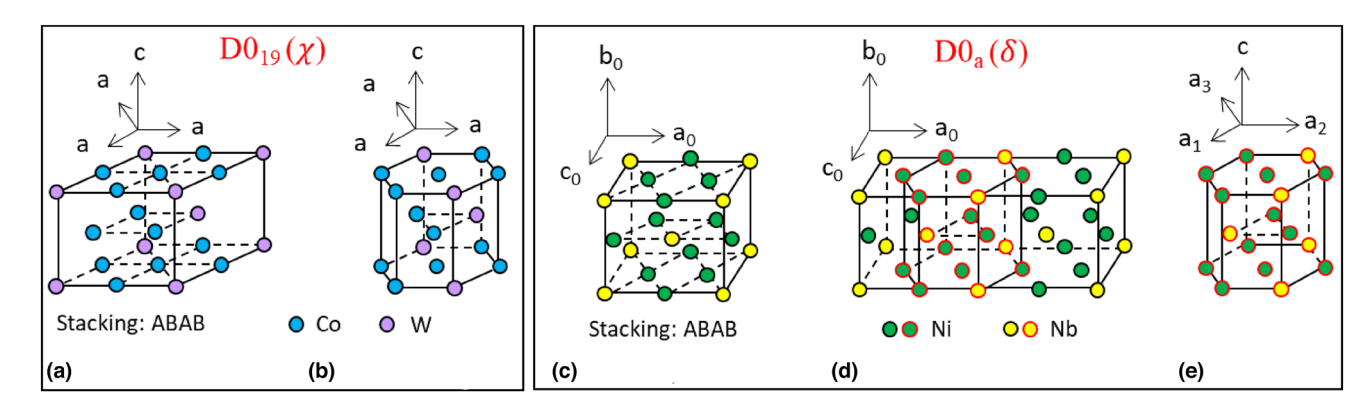


Figure 8. (a) $D0_{19}$ (χ) crystal structure with chemical prototype Co_3W . (b) HCP unit cell of $D0_{19}$ crystal structure. (c) Orthorhombic $D0_a$ (δ) crystal structure. (d) An HCP cell embedded in the orthorhombic unit cell for $D0_a$ (δ) crystal structure. (e) HCP cell comparable to (b) for $D0_a$ (δ) crystal structure.

Discover new LPT and SFPs

The second challenge is to discover new LPT and SFPs that could be beneficial for LPT-hardening. Our current understanding of the structure of SFPs are all based on their bulk counterparts, e.g., HCP for ISF, dHCP for ESF, χ for SISF, η for SESF, etc. But in the LPT mechanism, there is no requirement that the SFPs must be stable in bulk forms, or even exist in bulk form, just like the so-called grain boundary complexions.^[57] Even if SFPs have bulk counterparts, there can be more than one for a given stacking sequence. One obvious example is the crystal structure of D0₁₉ and D0_a, where both have the HCP stacking sequence but differ in their in-plane atomic ordering patterns. Figure 8 shows the crystal structure of D0₁₀ and D0_a. D0_a has an orthorhombic crystal structure [Fig. 8(c)] but there is an HCP-like cell embedded in the orthorhombic unit cell [Fig. 8(d)]. Comparing Figs. 8(b) and 6(e), it is clear that the ordering pattern is different, but both have the HCP stacking. It is even possible that in a multicomponent system D₀ is more stable than D0₁₉, which has not been considered yet, not to mention fault structures that do not have bulk counterpart and thus have not been taken into consideration. This is more important in alloys that are not FCC-based, where the stacking faults are not well characterized and understood. For instances, for HCP-based alloys, the basal slip would create local FCC stacking sequence, but non-basal slips could also create stacking faults that do not have well-define stacking sequences. The same can be said for BCC-based alloys and other low-symmetry alloys. Their structure states and compositional dependence of the stacking fault energy are largely missing from most current studies. This requires tremendous amounts of atomistic calculations and detailed experimental observations to complement each other, but the reward could be huge for the discovery of new alloys with greatly enhanced properties.

LPT kinetics

The discussion so far has been primarily on the thermodynamic understanding of LPTs. The kinetics of LPT is also important, especially for alloys under service at elevated temperatures. Since stacking faults are closely associated with the deformation process, there is a clear chemical-mechanical coupling that determines the kinetics of LPT. For instance, there is Cottrell atmosphere surrounding a dislocation at elevated temperatures, making the chemical environment around the dislocation different from the rest. Due to this change in the chemical environment, the critical stress for the dislocation to cut into a precipitate and create a stacking fault can differ. Moreover, while a fresh stacking fault is formed, it could quickly equilibrate and become the most stable SFP through atomic ordering/ reordering and disordering, and segregation or desegregation, all of which require atomic diffusion and the abundant solute atoms and excess atomic volume along the core of dislocations could provide a pathway for these processes to occur. Clearly, the segregation can have significantly impact on the energetics and kinetics of the formation of SFPs, which are dictated by

the diffusivity of solutes and the mobility of the dislocations. Microscopic phase field models (MPFM)^[58,59] informed by concentration-dependent generalized-stacking-fault (GSF) surfaces can be a great computational tool for this study. MPFM has been used to study precipitate shearing in various alloys systems without considering the concentration dependence of GSF. Various stacking fault configurations and deformation mechanisms have been investigated and excellent agreements have been achieved when compared with experiment observations. [40,60-63] If the concentration-dependent GSF is available, the dynamic chemical-mechanical coupling of the deformation processes could be studied in addition to the thermodynamic analysis. Mianroodi et al. [64] developed GSFs for both γ and γ' phases in a ternary Ni–Al–Co system as function of phase composition using molecular dynamics and conducted phase field simulations to demonstrate the effect of Co segregation on precipitate shearing. More effort is needed to consider other solutes, especially those related to the formation of different SFPs (like Cr and Nb), to understand not only the segregation but also the formation of SFPs.

Generality of LPT and its applications

Since defects have their own unique structures (different from the bulk phases that host them) and thus there are unique solute-defect interactions leading to LPTs. Besides the examples we have shown in this review, i.e., Ni-base superalloys where LPTs occur at not only stacking faults, but also at deformation twin boundaries, LPTs and metastable phases have also been found to be parts of deformation twin boundaries in shape memory alloys and metastable β -Ti alloys. [65] Furthermore, at interphase interfaces, significant solute segregation has also been observed in Al and Mg alloys. [66,67] These solutes can slow down significantly the coarsening process of the precipitates because the migration of the matrix/precipitate interface needs to drag the solutes with them. In micro-alloyed steels, interphase carbides are found to precipitate out at the interface between austenite and ferrite or austenite and pearlite, where the interphase interfaces act as preferred nucleation sites for the carbides. [68] At grain boundaries, various complexion transitions have been found and utilized to stabilize nanocrystalline materials.^[57,69] Similar complexions are also found at twin boundaries and dislocations as well.^[70] All the phenomena mentioned above share the same thermodynamic foundation, i.e., they are all enabled by the unique local defect structures at the extended defects and the corresponding solute-defect interactions.

Acknowledgments

The authors acknowledge the financial support from NSF DMREF program under grant DMR-1922239. LF and YW also thank Fan Zhang at CompuTherm for support of Pandat software and thermodynamic databases.



Data availability

The data that support the findings of this study are available from the corresponding author upon reasonable request.

Declarations

Conflict of interest

The authors declare that they have no known competing financial interests or personal relationships that could have appeared to influence the work reported in this paper.

References

- T.M. Smith, B.D. Esser, N. Antolin, A. Carlsson, R.E.A. Williams, A. Wessman, T. Hanlon, H.L. Fraser, W. Windl, D.W. McComb, Phase transformation strengthening of high-temperature superalloys. Nat. Commun. 7(1), 1 (2016)
- T.M. Smith, B.S. Good, T.P. Gabb, B.D. Esser, A.J. Egan, L.J. Evans, D.W. McComb, M.J. Mills, Effect of stacking fault segregation and local phase transformations on creep strength in Ni-base superalloys. Acta Mater. **172**, 55 (2019)
- A.J. Egan, Y. Rao, G.B. Viswanathan, T.M. Smith, M. Ghazisaeidi, S. Tin, M.J. Mills, Superalloys 2020 (Springer, New York, 2020), pp.640-650
- L. Feng, S.B. Kannan, A. Egan, T. Smith, M.J. Mills, M. Ghazisaeidi, Y. Wang, Localized phase transformation at stacking faults and mechanism-based alloy design. Acta Mater. (2022). https://doi.org/10.1016/j.actamat.2022. 118287
- T.M. Smith, B.D. Esser, N. Antolin, G.B. Viswanathan, T. Hanlon, A. Wessman, D. Mourer, W. Windl, D.W. McComb, M.J. Mills, Segregation and η phase formation along stacking faults during creep at intermediate temperatures in a Ni-based superalloy. Acta Mater. 100, 19 (2015)
- D. Barba, A. Egan, S. Kench, T.M. Smith, M.J. Mills, R.C. Reed, in TMS 2020 149th Annual Meeting & Exhibition Supplemental Proceedings (Springer, 2020), pp. 785-792
- R.E. Williams, T. Smith, B.D. Esser, N. Antolin, W. Windl, D.W. McComb, M.J. Mills, H.L. Fraser, Super-X EDS characterization of chemical segregation within a superlattice extrinsic stacking fault of a Ni-based superalloy. Microsc. Microanal. 21(S3), 493 (2015)
- T.M. Smith, N.A. Zarkevich, A.J. Egan, J. Stuckner, T.P. Gabb, J.W. Lawson, M.J. Mills, Utilizing local phase transformation strengthening for nickelbase superalloys. Commun. Mater. 2(1), 1 (2021)
- S.K. Makineni, A. Kumar, M. Lenz, P. Kontis, T. Meiners, C. Zenk, S. Zaefferer, G. Eggeler, S. Neumeier, E. Spiecker, On the diffusive phase transformation mechanism assisted by extended dislocations during creep of a single crystal CoNi-based superalloy. Acta Mater. 155, 362 (2018)
- S.K. Makineni, M. Lenz, S. Neumeier, E. Spiecker, D. Raabe, B. Gault, Elemental segregation to antiphase boundaries in a crept CoNi-based single crystal superalloy. Scripta Mater. 157, 62 (2018)
- 11. S.J. Pennycook, P.D. Nellist, Scanning Transmission Electron Microscopy: Imaging and Analysis (Springer, New York, 2011)
- Multiple: Scanning Transmission Electron Microscopy, 1st ed. (Springer, New York, 2011)
- M.K. Miller, M.G. Hetherington, Local magnification effects in the atom probe. Surf. Sci. 246(1-3), 442 (1991)
- T.M. Smith, B.D. Esser, B. Good, M.S. Hooshmand, G.B. Viswanathan, C.M.F. Rae, M. Ghazisaeidi, D.W. McComb, M.J. Mills, Segregation and phase transformations along superlattice intrinsic stacking faults in Nibased superalloys. Metall. Mater. Trans. A 49(9), 4186 (2018)
- L. Lilensten, S. Antonov, B. Gault, S. Tin, P. Kontis, Enhanced creep performance in a polycrystalline superalloy driven by atomic-scale phase transformation along planar faults. Acta Mater. 202, 232 (2021)
- B.H. Kear, A.F. Giamei, G.R. Leverant, J.M. Oblak, On intrinsic/extrinsic stacking fault pairs in the LI2 lattice. Scr. Metall. 3(2), 123 (1969)
- L. Kovarik, R.R. Unocic, J. Li, P. Sarosi, C. Shen, Y. Wang, M.J. Mills, Microtwinning and other shearing mechanisms at intermediate temperatures in Ni-based superalloys. Prog. Mater. Sci. 54(6), 839 (2009)

- 18. T.M. Smith, Y. Rao, Y. Wang, M. Ghazisaeidi, M.J. Mills, Diffusion processes during creep at intermediate temperatures in a Ni-based superalloy. Acta Mater. 141, 261 (2017)
- M.H.F. Sluiter, Y. Kawazoe, Site preference of ternary additions in \${\ mathrm{Ni}}_{3}\$Al. Phys. Rev. B 51(7), 4062 (1995)
- Q. Wu, S. Li, Alloying element additions to Ni3Al: Site preferences and effects on elastic properties from first-principles calculations. Comput. Mater. Sci. 53(1), 436 (2012)
- 21. C. Booth-Morrison, Z. Mao, R.D. Noebe, D.N. Seidman, Chromium and tantalum site substitution patterns in Ni3Al(L12) γ' -precipitates. Appl. Phys. Lett. 93(3), 033103 (2008)
- 22. L. Feng, Y. Rao, M. Ghazisaeidi, M.J. Mills, Y. Wang, Quantitative prediction of Suzuki segregation at stacking faults of the γ 'phase in Ni-base superalloys. Acta Mater. 200, 223 (2020)
- J. He, C.H. Zenk, X. Zhou, S. Neumeier, D. Raabe, B. Gault, S.K. Makineni, On the atomic solute diffusional mechanisms during compressive creep deformation of a Co-Al-W-Ta single crystal superalloy. Acta Mater. 184, 86 (2020)
- 24. M.S. Titus, A. Mottura, G.B. Viswanathan, A. Suzuki, M.J. Mills, T.M. Pollock, High resolution energy dispersive spectroscopy mapping of planar defects in L12-containing Co-base superalloys. Acta Mater. 89, 423
- 25. Y.M. Eggeler, M.S. Titus, A. Suzuki, T.M. Pollock, Creep deformationinduced antiphase boundaries in L12-containing single-crystal cobaltbase superalloys. Acta Mater. 77, 352 (2014)
- M.S. Titus, R.K. Rhein, P.B. Wells, P.C. Dodge, G.B. Viswanathan, M.J. Mills, A. Van der Ven, T.M. Pollock, Solute segregation and deviation from bulk thermodynamics at nanoscale crystalline defects. Sci. Adv. 2(12), e1601796 (2016)
- 27. M.S. Titus, Y.M. Eggeler, A. Suzuki, T.M. Pollock, Creep-induced planar defects in L12-containing Co-and CoNi-base single-crystal superalloys. Acta Mater. 82, 530 (2015)
- X. Wu, A. Dlouhy, Y.M. Eggeler, E. Spiecker, A. Kostka, C. Somsen, G. Eggeler, On the nucleation of planar faults during low temperature and high stress creep of single crystal Ni-base superalloys. Acta Mater. 144, 642 (2018)
- Y.M. Eggeler, J. Müller, M.S. Titus, A. Suzuki, T.M. Pollock, E. Spiecker, Planar defect formation in the γ' phase during high temperature creep in single crystal CoNi-base superalloys. Acta Mater. 113, 335 (2016)
- S. Lu, S. Antonov, L. Li, C. Liu, X. Zhang, Y. Zheng, H.L. Fraser, Q. Feng, Atomic structure and elemental segregation behavior of creep defects in a Co-Al-W-based single crystal superalloys under high temperature and low stress. Acta Mater. 190, 16 (2020)
- 31. F.L.R. Tirado, J.P. Toinin, D.C. Dunand, $\gamma + \gamma'$ microstructures in the Co-Ta-V and Co-Nb-V ternary systems. Acta Mater. 151, 137 (2018)
- J.W. Cahn, Critical point wetting. J. Chem. Phys. 66(8), 3667 (1977)
- N. Ma, S.A. Dregia, Y. Wang, Solute segregation transition and drag force on grain boundaries. Acta Mater. 51(13), 3687 (2003)
- N. Ma, C. Shen, S.A. Dregia, Y. Wang, Segregation and wetting transition at dislocations. Metall. Mater. Trans. A 37(6), 1773 (2006)
- P. Wynblatt, D. Chatain, Solid-state wetting transitions at grain boundaries. Mater. Sci. Eng. A 495(1-2), 119 (2008)
- H. Suzuki, Segregation of solute atoms to stacking faults. J. Phys. Soc. Jpn. 17(2), 322 (1962)
- H. Suzuki, Chemical interaction of solute atoms with dislocations. Sci. Rep. Res. Inst. 4, 455 (1952)
- C.M.F. Rae, R.C. Reed, Primary creep in single crystal superalloys: origins, mechanisms and effects. Acta Mater. 55(3), 1067 (2007)
- 39. Y.M. Eggeler, K.V. Vamsi, T.M. Pollock, Precipitate shearing, fault energies, and solute segregation to planar faults in Ni-, CoNi-, and Co-base superalloys. Annu. Rev. Mater. Res. 51, 209 (2021)
- 40. V.A. Vorontsov, C. Shen, Y. Wang, D. Dye, C.M.F. Rae, Shearing of γ' precipitates by a< 1 1 2> dislocation ribbons in Ni-base superalloys: a phase field approach. Acta Mater. 58(12), 4110 (2010)
- T.M. Smith, T.P. Gabb, K.N. Wertz, J. Stuckner, L.J. Evans, A.J. Egan, M.J. Mills, Superalloys 2020 (Springer, New York, 2020), pp.726-736
- Y. Wen, S.U.N. Jian, J. Huang, First-principles study of stacking fault energies in Ni3Al intermetallic alloys. Trans. Nonferrous Met. Soc. China 22(3), 661 (2012)

Computational Approaches for Materials Discovery and Development Prospective

- 43. K. Kumar, R. Sankarasubramanian, U.V. Waghmare, Influence of dilute solute substitutions in Ni on its generalized stacking fault energies and ductility. Comput. Mater. Sci. 150, 424 (2018)
- 44. K. Kumar, R. Sankarasubramanian, U.V. Waghmare, Tuning planar fault energies of Ni3Al with substitutional alloying: first-principles description for guiding rational alloy design. Scripta Mater. 142, 74 (2018)
- 45. K.V. Vamsi, S. Karthikeyan, Effect of off-stoichiometry and ternary additions on planar fault energies in Ni3Al. Superalloys 2012(1), 521 (2012)
- 46. H. Hasan, P. Mikvik, P.D. Haynes, V.A. Vorontsov, Generalised stacking fault energy of Ni-Al and Co-Al-W superalloys: density-functional theory calculations. Materialia 9, 100555 (2020)
- 47. A. Breidi, J. Allen, A. Mottura, First-principles modeling of superlattice intrinsic stacking fault energies in Ni3Al based alloys. Acta Mater. 145,
- C. Hu, Z. Zhang, H. Chen, J. He, H. Guo, Reactive elements dependence of elastic properties and stacking fault energies of γ -Ni, γ' -Ni3Al and β-NiAl. J. Alloys Compds. 843, 155799 (2020)
- 49. W. Yang, P. Qu, J. Sun, Q. Yue, H. Su, J. Zhang, L. Liu, Effect of alloying elements on stacking fault energies of γ and γ' phases in Ni-based superalloy calculated by first principles. Vacuum 181, 109682 (2020)
- 50. X.-X. Yu, C.-Y. Wang, The effects of alloying elements on generalized stacking fault energies, strength and ductility of $\gamma^\prime\textsc{-Ni3Al}.$ Mater. Sci. Eng. A 539, 38 (2012)
- 51. G. Ceder, K. Persson: The Materials Project: A Materials Genome Approach (2010)
- K.V. Vamsi, T.M. Pollock, A new proximate structure for the APB (111) in L12 compounds. Scripta Mater. 182, 38 (2020)
- 53. M. Wang, H.L. Yu, Y. Chen, M.X. Huang, Machine learning assisted screening of non-rare-earth elements for Mg alloys with low stacking fault energy. Comput. Mater. Sci. 196, 110544 (2021)
- 54. X. Chong, S.-L. Shang, A.M. Krajewski, J.D. Shimanek, W. Du, Y. Wang, J. Feng, D. Shin, A.M. Beese, Z.-K. Liu, Correlation analysis of materials properties by machine learning: illustrated with stacking fault energy from first-principles calculations in dilute fcc-based alloys. J. Phys.: Condens. Matter 33(29), 295702 (2021)
- G. Arora, D.S. Aidhy, Machine learning enabled prediction of stacking fault energies in concentrated alloys. Metals 10(8), 1072 (2020)
- X. Wang, W. Xiong, Stacking fault energy prediction for austenitic steels: thermodynamic modeling vs. machine learning. Sci. Technol. Adv. Mater. 21(1), 626 (2020)
- P.R. Cantwell, M. Tang, S.J. Dillon, J. Luo, G.S. Rohrer, M.P. Harmer, Grain boundary complexions. Acta Mater. 62, 1 (2014)

- 58. Y.U. Wang, Y.M. Jin, A.M. Cuitino, A.G. Khachaturyan, Nanoscale phase field microelasticity theory of dislocations: model and 3D simulations. Acta Mater. 49(10), 1847 (2001)
- C. Shen, Y. Wang, Phase field model of dislocation networks. Acta Mater. 51(9), 2595 (2003)
- 60. L. Feng, D. Lv, R.K. Rhein, J.G. Goiri, M.S. Titus, A. Van der Ven, T.M. Pollock, Y. Wang, Shearing of γ ' particles in Co-base and Co-Ni-base superalloys. Acta Mater. 161, 99 (2018)
- 61. C.H. Zenk, L. Feng, D. McAllister, Y. Wang, M.J. Mills, Shearing mechanisms of co-precipitates in IN718. Acta Mater. 220, 117305 (2021)
- D.C. Lv, D. McAllister, M.J. Mills, Y. Wang, Deformation mechanisms of D022 ordered intermetallic phase in superalloys. Acta Mater. 118, 350
- 63. N. Zhou, C. Shen, M.J. Mills, J. Li, Y. Wang, Modeling displacive-diffusional coupled dislocation shearing of γ' precipitates in Ni-base superalloys. Acta Mater. **59**(9), 3484 (2011)
- 64. J.R. Mianroodi, P. Shanthraj, P. Kontis, J. Cormier, B. Gault, B. Svendsen, D. Raabe, Atomistic phase field chemomechanical modeling of dislocationsolute-precipitate interaction in Ni-Al-Co. Acta Mater. 175, 250 (2019)
- Y.P. Gao, Y.F. Zheng, D. Wang, H.L. Fraser, Y. Wang: Extended twin boundary structure and symmetry-dictated deformation path in a titanium alloys. Acta Mater. (n.d.)
- 66. Y. Ou, Y. Jiang, Y. Wang, Z. Liu, A. Lervik, R. Holmestad, Vacancy and solute co-segregated $\eta 1$ interface in over-aged Al-Zn-Mg alloys. Acta Mater. **218**, 117082 (2021)
- 67. Y. Zheng, Y. Liu, N. Wilson, S. Liu, X. Zhao, H. Chen, J. Li, Z. Zheng, L. Bourgeois, J.-F. Nie, Solute segregation induced sandwich structure in Al-Cu (-Au) alloys. Acta Mater. 184, 17 (2020)
- 68. F.A. Khalid, D.V. Edmonds, Interphase precipitation in microalloyed engineering steels and model alloy. Mater. Sci. Technol. 9(5), 384 (1993)
- 69. W.D. Kaplan, D. Chatain, P. Wynblatt, W.C. Carter, A review of wetting versus adsorption, complexions, and related phenomena: the rosetta stone of wetting. J. Mater. Sci. 48(17), 5681 (2013)
- M. Kuzmina, M. Herbig, D. Ponge, S. Sandlöbes, D. Raabe, Linear complexions: confined chemical and structural states at dislocations. Science **349**(6252), 1080 (2015)

Springer Nature or its licensor holds exclusive rights to this article under a publishing agreement with the author(s) or other rightsholder(s); author self-archiving of the accepted manuscript version of this article is solely governed by the terms of such publishing agreement and applicable law.